

Far Infrared Synchrotron Near-Field Nanoimaging and Nanospectroscopy

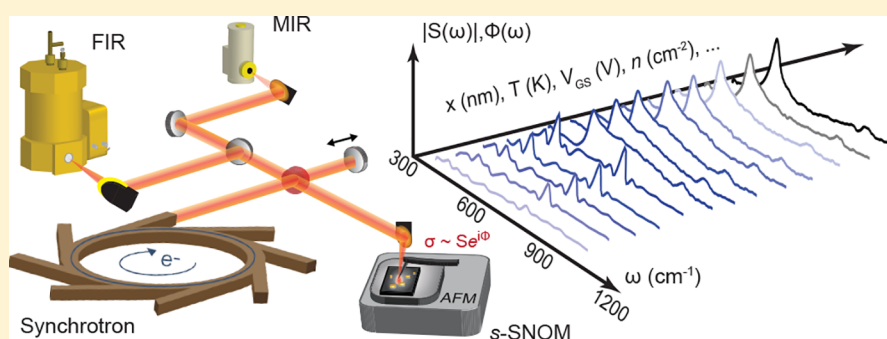
Omar Khatib,^{†,‡,§} Hans A. Bechtel,^{*,‡} Michael C. Martin,[‡] Markus B. Raschke,^{*,†,§} and G. Lawrence Carr^{*,§}

[†]Department of Physics, Department of Chemistry, and JILA, University of Colorado, Boulder, Colorado 80309, United States

[‡]Advanced Light Source Division, Lawrence Berkeley National Laboratory, Berkeley, California 94720, United States

[§]National Synchrotron Light Source II, Brookhaven National Laboratory, Upton, New York 11973, United States

Supporting Information



ABSTRACT: Scattering scanning near-field optical microscopy (*s*-SNOM) has emerged as a powerful imaging and spectroscopic tool for investigating nanoscale heterogeneities in biology, quantum matter, and electronic and photonic devices. However, many materials are defined by a wide range of fundamental molecular and quantum states at far-infrared (FIR) resonant frequencies currently not accessible by *s*-SNOM. Here we show ultrabroadband FIR *s*-SNOM nanoimaging and spectroscopy by combining synchrotron infrared radiation with a novel fast and low-noise copper-doped germanium (Ge:Cu) photoconductive detector. This approach of FIR synchrotron infrared nanospectroscopy (SINS) extends the wavelength range of *s*-SNOM to 31 μm (320 cm^{-1} , 9.7 THz), exceeding conventional limits by an octave to lower energies. We demonstrate this new nanospectroscopic window by measuring elementary excitations of exemplary functional materials, including surface phonon polariton waves and optical phonons in oxides and layered ultrathin van der Waals materials, skeletal and conformational vibrations in molecular systems, and the highly tunable plasmonic response of graphene.

KEYWORDS: far-infrared, near-field microscopy, *s*-SNOM, synchrotron infrared nanospectroscopy, graphene plasmonics, spatio-spectral nanoimaging

Near-field nanoscopy attracts increasing scientific attention, specifically in the implementation of infrared scattering type scanning near-field optical microscopy (IR *s*-SNOM).^{1–4} It provides for nanoimaging and nanospectroscopy down to a few nanometer length scales, gaining insight into molecular orientation⁵ and coupling,⁶ catalytic activity,⁷ heterogeneity in electron and lattice dynamics,^{8,9} and plasmonic and polaritonic effects in quantum matter^{10–13} with recent extension to the low temperature^{9,14} and ultrafast regimes.^{15–18} Despite these significant developments, *s*-SNOM has largely been limited to a narrow range of the electromagnetic spectrum of the near- to mid-IR at high frequencies, and the RF¹⁹ and low THz²⁰ regime at low frequencies.

However, the far-infrared (FIR) and lower mid-infrared (MIR) spectral range ($10\text{--}700\text{ cm}^{-1}$, $14\text{--}1000\text{ }\mu\text{m}$, $0.3\text{--}20\text{ THz}$, $3\text{--}190\text{ K}$) has yet remained largely unexplored in *s*-SNOM, despite the significance of its low-energy molecular and quantum state resonances that define material functions from

condensed matter physics to biology and medicine. Many fundamental excitations and collective modes in solids have characteristic energies in the FIR, including the free carrier Drude response, crystal lattice vibrations, charge density waves, superconducting energy gaps, magnetic excitations, surface plasmon and phonon polaritons, and others (Figure 1a).²¹ Similarly, in soft and biological molecular materials, the FIR provides spectral access to structurally specific (“fingerprint”) vibrations and conformations via skeletal, torsional, and deformation modes, that allow for direct probing of, for example, the secondary structure of proteins.²²

The extension of *s*-SNOM into the FIR range has largely been hampered by the lack of both suitable light sources and detectors. On the high frequency side, IR *s*-SNOM is performed with different femtosecond laser based super-

Received: April 30, 2018

Published: May 11, 2018

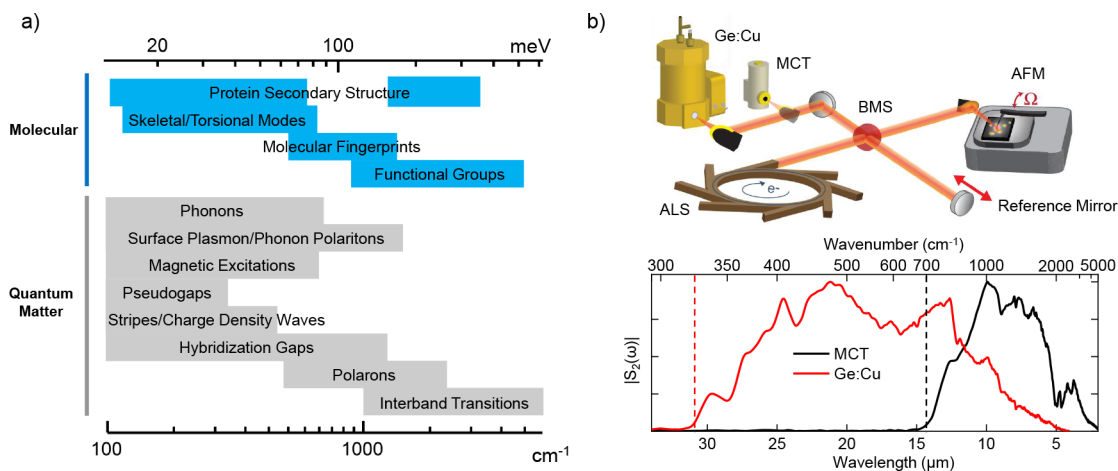


Figure 1. (a) Infrared energy scales and associated phenomena in molecular and quantum matter; (b) Top: ultrabroadband SINS experimental configuration with extension to far-infrared frequencies; bottom: SINS reference spectrum using MCT (black curve) and Ge:Cu (red curve) detectors, demonstrating extended near-field spectroscopic performance at frequencies down to 320 cm^{-1} .

continuum and parametric generation sources for broadband or broadly tunable mid-IR radiation, yet limited by suitable nonlinear optical crystals for frequency conversion to wavelengths $<18\ \mu\text{m}$.²³ At low frequencies, THz *s*-SNOM nanoimaging is performed with continuous wave THz sources, such as gas lasers and QCLs at a limited number of fixed frequencies,^{20,24} or with broadband THz light generated from photoconductive antennas, limited to $<3\text{ THz}$ ^{25–27} and low power output.

To date, far-IR *s*-SNOM has only routinely been achieved using a free electron laser (FEL) that provides the necessary high intensity quasi-cw radiation as needed for *s*-SNOM.^{28,29} Although in principle continuously tunable from 1.5–75 THz ($50\text{--}2500\text{ cm}^{-1}$, $4\text{--}200\ \mu\text{m}$), for *s*-SNOM nanospectroscopy, a broadband FIR light source with simultaneous high bandwidth and spectral irradiance across a broad spectral range would be most desirable. Not only does this enable signal multiplexing and self-referencing to eliminate noise and systematic errors, but it also allows for the simultaneous probing of multiple characteristic material resonances, as desirable in monitoring kinetics of phase transitions or chemical transformations on the nanoscale.

In addition to limitations in the availability of suitable light sources is a lack of far-infrared detectors with the necessary speed and sensitivity for FIR *s*-SNOM. Mid-IR detectors based on small bandgap semiconductor alloys, such as $\text{Hg}_{1-x}\text{Cd}_x\text{Te}$ (MCT), have a long-wavelength cutoff typically at 600 cm^{-1} , with extension to lower frequency at the expense of drastically reduced sensitivity and challenged by material limitations. On the other hand, conventional FIR detectors such as pyroelectric deuterated triglycine sulfate (DTGS) or liquid helium cooled Si bolometers only operate at $< \text{few kHz}$ frequencies and have too slow response times. Extrinsic impurity photoconductors based on doped Si or Ge offer fast intrinsic response times ($<100\text{ ns}$) and small bandgaps in the FIR, yet in their usual implementation are plagued by excess thermal background and electronic noise, rendering them unsuitable for *s*-SNOM (see Supporting Information for extended discussion).

In this Letter, we demonstrate ultrabroadband near-field nanospectroscopy covering the qualitatively new regime of far-IR *s*-SNOM. We utilize synchrotron radiation, which provides a low-noise, broadband, and coherent light source with high spectral irradiance at frequencies spanning from THz to the

extreme UV region.³⁰ To detect the tip-scattered near-field FIR signal we have developed a custom, MHz bandwidth Ge:Cu photoconductor with superior sensitivity for spectroscopic FIR *s*-SNOM nanoimaging. With this approach we are able to extend the wavelength range of *s*-SNOM by one octave, overcoming conventional limits, down to $31\ \mu\text{m}$ (320 cm^{-1}).

To demonstrate the performance in this new spectral regime, we probe previously inaccessible types of excitations with far-IR *s*-SNOM. This includes low energy phonons in anisotropic bulk crystalline media, as well as layered van der Waals systems, of interest for potential nanophotonics applications as natural hyperbolic materials. Skeletal deformations and torsional modes in organic semiconductor films allow for the simultaneous nanoprobng of several vibrational degrees of freedom in molecular materials, which heavily influence the low energy electronic and transport properties of functional devices. We access the THz plasmonic regime in graphene, including plasmon–phonon substrate interactions, and demonstrate a high degree of gate tunability. Lastly, we provide a platform to extend to yet longer wavelengths by combining with other extrinsic Ge detectors.

Figure 1b displays a schematic of the ultrabroadband *s*-SNOM nanospectroscopy implementation, based on an atomic force microscope (AFM) using metal-coated tips, and interferometric detection as described previously.³⁰ IR synchrotron radiation is provided by the Advanced Light Source (ALS) at Lawrence Berkeley National Laboratory in two experimental configurations: Beamline 5.4, employing a specially modified AFM (Innova, Bruker) coupled to a commercial FTIR Spectrometer (Nicolet 6700, Thermo-Scientific), and Beamline 2.4 using a commercial nanoscope (neaSNOM, Neaspec GmbH), to measure the spectral near-field scattering amplitude and phase response $|S(\omega)|e^{i\Phi(\omega)}$. As a direct probe of the sample dielectric function, broadband *s*-SNOM amplitude and phase typically exhibit simple dispersive and absorptive lineshapes, respectively, for weaker oscillators, and a more complicated hybrid response for strongly resonant and collective excitations.^{23,31} The customized LHe-cooled Ge:Cu detector for synchrotron infrared nanospectroscopy (SINS) provides a broadband response ($2\text{--}31\ \mu\text{m}$) and suitable sensitivity ($D^* > 10^{10}\text{ cm}\cdot\sqrt{\text{Hz}}/\text{W}$). The low energy cutoff of Ge:Cu of $31\ \mu\text{m}$ (320 cm^{-1}), limited by impurity band

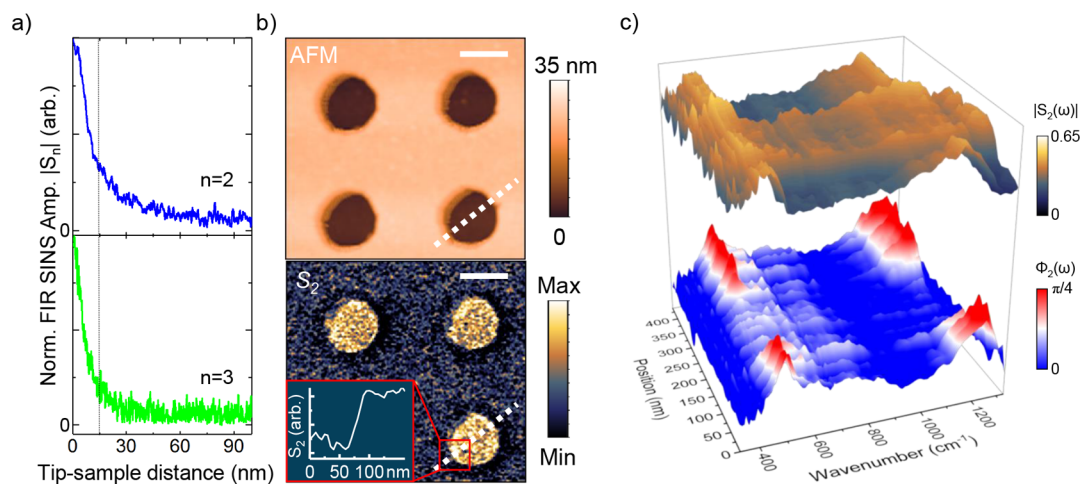


Figure 2. FIR *s*-SNOM spatio-spectral characteristics. (a) Tip–sample distance dependence in second (blue trace) and third (green trace) order demodulation of the tip tapping frequency (75–300 kHz). (b) Far-IR nanoimaging of 25 nm-thick SiO₂ hole array, with AFM topography (top), and spectrally integrated SINS amplitude signal S_2 (bottom), demonstrating near-field contrast between the patterned SiO₂ and underlying Si substrate with \sim 30 nm spatial resolution (inset). Scale bar is 200 nm. (c) Spatio-spectral line scan (450 nm \times 40 px) with trajectory indicated by dotted line in (b), showing broadband SINS amplitude $S_2(\omega)$ (top) and phase $\Phi_2(\omega)$ (bottom) of asymmetric Si–O bend (460 cm⁻¹) and stretch (1200 cm⁻¹) phonon bands in SiO₂.

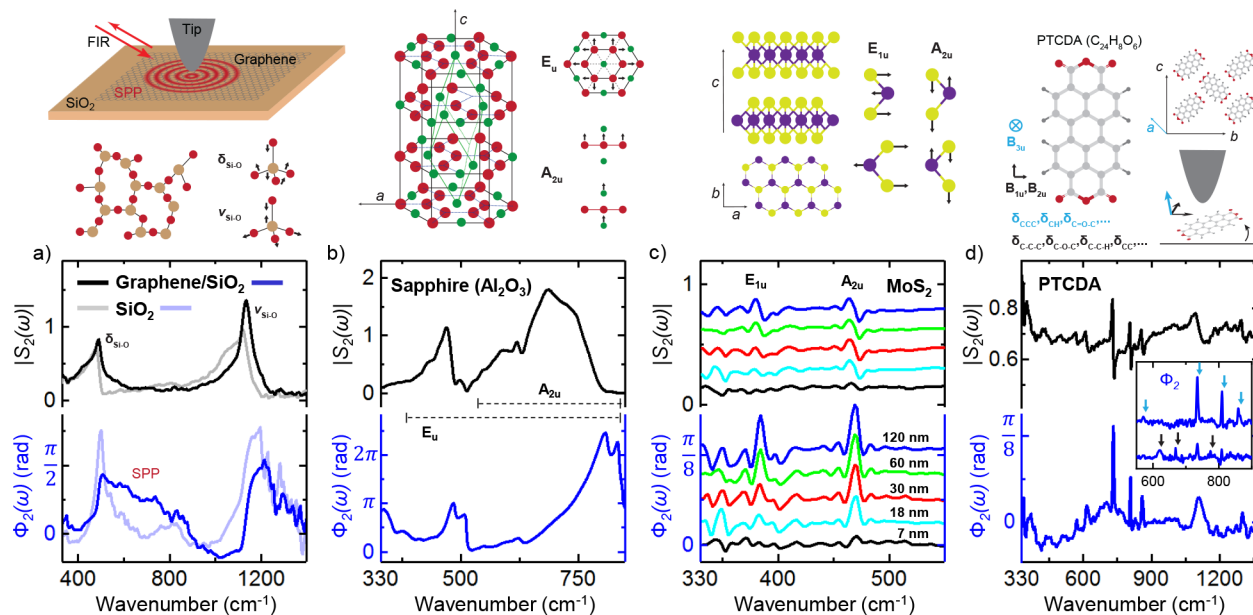


Figure 3. FIR SINS amplitude $|S_2(\omega)|$ (top curves) and phase $\Phi_2(\omega)$ (bottom curves) spectra of selected material systems. (a) SiO₂ with (dark traces) and without (light traces) a graphene overlayer, showing graphene plasmon-induced modification of the FIR near-field response. (b) Low energy E_u and A_{2u} phonon bands for strongly resonant c-cut sapphire. (d) Thickness-dependent E_{1u} in-plane and A_{2u} out-of-plane optical phonons of layered van der Waals material MoS₂. (d) Molecular semiconductor PTCDA, showing vibrational modes from skeletal deformations in the IR fingerprint range. Inset compares $\Phi_2(\omega)$ for two adjacent crystal grains with differing orientation, with the respective IR-active modes indicated by arrows. Cartoon schematics above data panels depict the resonant excitations probed by the tip.

transitions from the Ge valence band edge, represents over a factor of 2 extension in wavelength compared to conventional MCTs (bottom panel in Figure 1b). Complete details of the experimental setup, measurements, and Cu:Ge detector can be found in the Supporting Information.

We first demonstrate the ultrahigh nanometer spatial resolution capability of FIR *s*-SNOM in SINS. Figure 2a,b shows the vertical and lateral field localization, respectively, of FIR synchrotron radiation by the AFM tip. *s*-SNOM approach curves (Figure 2a) at second and third order tip demodulation (see Supporting Information) demonstrate the few-nm confine-

ment of the long wavelength tip-scattered light. Figure 2b shows a 1 μ m² image of a patterned SiO₂/Si test sample with AFM topography (top) and spectrally integrated FIR SINS amplitude $|S_2|$ (bottom), revealing strong dielectric contrast between SiO₂ and Si with \sim 30 nm spatial resolution (Figure 2b, inset), corresponding to $\lambda/1100$.

Figure 2c shows a nanospatospectral line scan, reflecting the real and imaginary spectral dielectric response across a 200 nm hole in SiO₂, indicated by the white dotted line in Figure 2b and normalized to a Au reference. The spectral features are the surface optical phonon polaritons of SiO₂, due to the

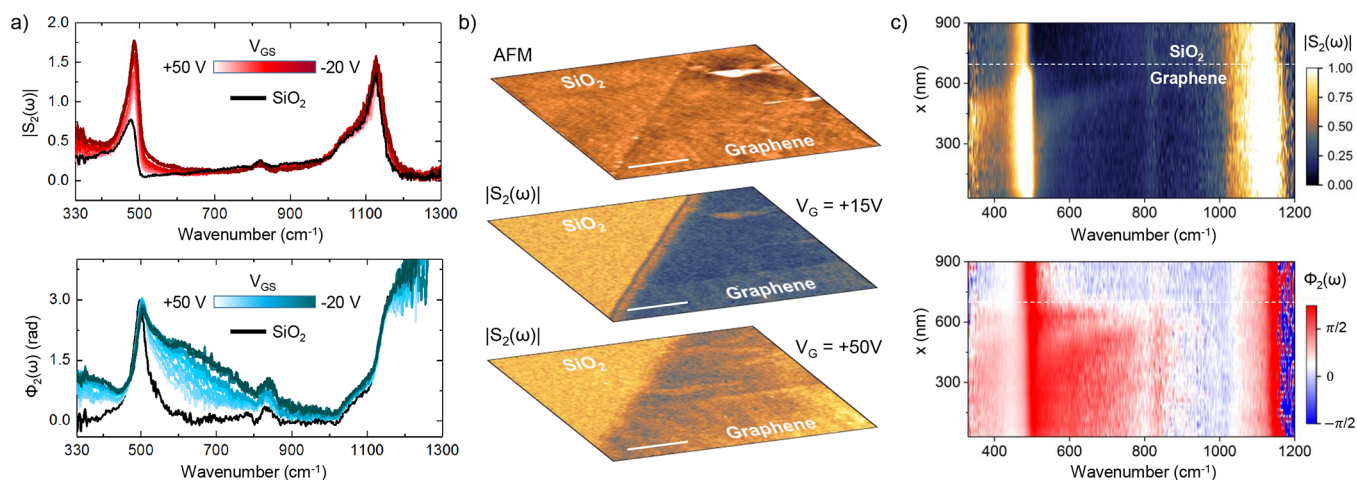


Figure 4. Far-IR graphene plasmonics. (a) Gate-tuning of SINS amplitude $|S_2(\omega)|$ (red shaded curves) and phase $\Phi_2(\omega)$ (blue shaded curves) for a functional graphene device on SiO_2 (black line), showing modulation of free carrier Drude response and plasmon absorption in graphene. (b) SINS nanoimaging of graphene/ SiO_2 interface for highly doped ($V_{GS} = +15\text{ V}$, middle panel) and low-doped ($V_{GS} = +50\text{ V}$, bottom panel) graphene. Scale bar is $1\ \mu\text{m}$. (c) SINS spatio-spectral line scan across doped-graphene/ SiO_2 boundary, demonstrating nanometer broadband spectroscopic access to far-IR surface plasmon polariton (SPP) waves in graphene down to $320\ \text{cm}^{-1}$. The SPP dispersion as a function of energy can be observed directly near the graphene edge, where reflected surface waves constructively interfere with those launched from the AFM tip.

asymmetric Si–O stretch vibration near $1200\ \text{cm}^{-1}$,³¹ and the previously inaccessible $460\ \text{cm}^{-1}$ asymmetric Si–O bending mode.³² This low energy mode is especially important for coupling to far-IR surface plasmons in ultrathin materials (see below) and highlights the ability of SINS for simultaneous probing of multiple spectrally separated material resonances with $<30\ \text{nm}$ spatial resolution.

We present additional FIR SINS spectra of representative classes of other material systems in Figure 3, which exhibit important low energy resonant features. Figure 3a first shows the FIR SINS spectra of SiO_2 with and without an ultrathin single sheet of graphene on top. The presence of monolayer graphene significantly modifies the local FIR response, with increased absorption as seen in the near-field phase, due to the excitation and strong interaction between graphene plasmons and SiO_2 substrate phonons that we explore in more detail below. Strong light-matter interactions in the near-field for polar dielectrics and other crystalline materials can result in very large scattering amplitudes exceeding highly reflective nonresonant surfaces such as Au. Figure 3b shows the reststrahlen region of *c*-cut sapphire (Al_2O_3) for its E_u and A_{2u} optical phonon branches, covering the range where its hyperbolic response arises from an intrinsic optical anisotropy.³³

Using FIR SINS, we have the sensitivity to even probe weak excitations in layered and molecular materials. Figure 3c shows van der Waals material MoS_2 , with its A_{2u} out-of-plane mode at $468\ \text{cm}^{-1}$ and E_{1u} in-plane mode³⁴ at $384\ \text{cm}^{-1}$ for a number of exfoliated flakes of different thicknesses. We are able to discern these phonon features for MoS_2 layers down to $7\ \text{nm}$ in thickness, demonstrating a unique symmetry sensitivity, even in layered systems with small interlayer coupling. FIR SINS can also be used as an orientational probe in molecular solids. Figure 3d shows a range of skeletal and deformation modes in the aromatic ring structure of organic semiconductor perylenetetracarboxylic dianhydride (PTCDA), including both in-plane (B_{1u} , B_{2u}) and out-of-plane (B_{3u}) bending vibrations (e.g., $\delta_{\text{C-C-C}}$, $\delta_{\text{C=O-C}}$, etc.),³⁵ for a relatively uniform, thick film. The relative intensity of these modes can be used to map the

spatial distribution at the single crystallite level,⁵ as seen by comparing two adjacent PTCDA grains within a few hundred nanometers in a more heterogeneous area of the sample (Figure 3d, inset).

Investigation of molecular and low-dimensional materials often necessitates controlled modification of external parameters. Graphene attracts much attention because of its inherently tunable IR and THz plasmonic response, as well as its extreme sensitivity to local interactions and coupling to the underlying substrate. Figure 4a demonstrates modulation of the far-IR SINS signal of a functional graphene/ SiO_2 device subject to in situ electrostatic tuning of the back gate voltage V_{GS} . We observe a significant modification of the far-IR response with gate bias, with a strong enhancement of both $|S_2(\omega)|$ (top, red shaded curves) and $\Phi_2(\omega)$ (bottom, blue shaded curves) for negative voltages, and a nearly full suppression for high positive voltages above $+50\ \text{V}$, approaching the intrinsic response of the underlying SiO_2 (black curve).

The voltage-dependent response of graphene additionally displays strong far-IR contrast in spectrally integrated SINS nanoimaging (Figure 4b), with a bright stripe within few hundred nm of the graphene/ SiO_2 edge at low gate bias (middle panel), whereas at higher voltage the image contrast weakens and becomes more uniform with the adjacent SiO_2 substrate (bottom panel). Also evident is a significant degree of nanoscale heterogeneity in the FIR contrast, indicative of doping variations across the graphene flake likely related to a distribution of charged impurities trapped at the interface with the underlying SiO_2 substrate.

Lastly, Figure 4c reveals a rich spectral structure in $|S_2(\omega)|$ and $\Phi_2(\omega)$ confined to within $300\ \text{nm}$ of the graphene/ SiO_2 interface, yet probed at far-IR wavelengths down to $31\ \mu\text{m}$. The spectral response observed is the result of gate-tuning of the free carrier Drude response in graphene, superimposed with the excitation of surface plasmon polariton (SPP) waves that are launched by the metallic probe tip, and propagate radially away and interfere with reflected waves from the graphene/ SiO_2 edge, observed previously in monochromatic mid-IR *s*-SNOM nanoimaging.^{10,11,36} The SPP dispersion as a function of energy

can readily be observed near the graphene interface, with the polariton wavelength determined by the distance of the modulated near-field amplitude and phase from the edge. The spectral behavior and enhancement near the SiO₂ resonances indicates a hybridization and strong coupling between graphene SPPs and substrate surface phonons. The observation of only a single polariton branch is likely due to a strong damping of the plasmons, common for graphene on SiO₂, not encapsulated in hBN,³⁷ because of a high density of charged impurity scatterers, the effect of which is seen in Figure 4b.

This direct nanospectroscopic visualization of the coupled plasmon–phonon dispersion spans a spectral range four times as large as previous *s*-SNOM work on graphene plasmons,³⁸ covering multiple coupled substrate phonon resonances and for the first time including the lower FIR plasmonic branch of graphene. The combined data in Figure 4 thus demonstrate expansion into the FIR plasmon tuning range of graphene, opening a new regime in this and related 2D materials.

The material responses probed in this work demonstrate the capability of FIR SINS for new scientific investigations previously unavailable in *s*-SNOM. The low energy optical phonon regime in solids is critical to studies ranging from thermal transport and electron–phonon scattering in low dimensional materials³⁹ to mediating interactions in strongly correlated materials and superconductors.⁴⁰ The wide spectral coverage of FIR SINS allows for simultaneous nanoprobng of free carriers in weakly metallic systems and other collective modes such as magnetic or charge density wave excitations.²¹ Additionally, the high sensitivity to weak flexural and torsional modes in molecular materials (Figure 3d) can be used to disentangle competing effects in for example organic semiconductors. In these systems, charge dynamics are dominated by a complex interplay of structural and vibrational nanoscale disorder, giving rise to localized excitations such as polarons.⁴¹

The promise of tunable graphene plasmonics is already being exploited for the development of novel nanophotonics applications from visible to THz frequencies.⁴² In this atomically thin sheet of carbon, there is great interest in coupling plasmons to other vibrations in adjacent layers or substrates, given its high sensitivity to the immediate environment.⁴³ As seen in Figure 4, with FIR SINS we observe a significant 3-fold enhancement of the low energy SiO₂ phonon mode and direct absorption of graphene plasmons, suggesting a very strong plasmon-phonon coupling that is more sensitively tunable with gating compared to the higher energy mode. This also opens up new opportunities for studying a wide range of corresponding modes in 2D and Dirac materials, including transition metal dichalcogenides, black phosphorus, and topological insulators, which typically host plasmons at FIR energies.¹³ Further, large intrinsic anisotropies in these and other polar dielectric crystals can be explored for use as natural hyperbolic materials for unique nanophotonics applications in the FIR, without the need for artificial metamaterials with high losses,⁴⁴ all with nanoscale spatial resolution.

Our approach can be further extended toward lower THz frequencies below 300 cm⁻¹, for example by choosing other Ge or Si impurity conductors such as Ge:Zn (2–40 μm) or Ge:Ga (30–100 μm), which was recently used in FIR *s*-SNOM nanoimaging using a high-power FEL,^{28,29} yet could be improved in sensitivity using our electronic modifications. While conventional helium-cooled Si bolometers, which are typically used for far-IR measurements in the far-field, have the

necessary sensitivity (NEP < pW/Hz^{0.5}) and spectral bandwidth (10–1000 cm⁻¹), they are exceedingly slow in their standard configuration with detection speeds of <1 kHz. Superconducting hot electron bolometers offer another possibility for this spectral range, with sufficient speed and broadband coverage from 30–1000 cm⁻¹, but sensitivity is often limited to ~10 pW/Hz^{0.5}. Recent antenna-coupled Nb bolometers, however, have demonstrated sub-ns response times and a NEP of 20 fW/Hz^{0.5}.⁴⁵ Alternative detection schemes such as nonsynchronized electro-optic sampling, which directly measures the electric field, have also been shown to be compatible for continuous wave sources up to 40 THz.⁴⁶ Lastly, we believe detector electronics can be yet improved to further reduce electronic noise, ultimately achieving photon noise-limited detection (see Supporting Information for extended discussion).

In conclusion, we have demonstrated a qualitatively new regime of IR *s*-SNOM nanoimaging and nanospectroscopy through far-infrared SINS. Utilizing the spatial coherence, high spectral irradiance, and ultrabroadband properties of synchrotron IR radiation, combined with a custom low-noise fast modulating Ge:Cu photoconductor, we are able to provide nanospectroscopic capabilities to wavelengths down to 31 μm (320 cm⁻¹) with ultrahigh 30 nm spatial resolution. We demonstrate unique spatio-spectral access to a range of resonant far-IR electronic and lattice excitations, including the low-energy free carrier response, surface phonon polariton waves and optical phonons in oxides and ultrathin van der Waals materials, skeletal deformations and conformational vibrations in molecular systems, and the highly tunable FIR plasmonic regime of graphene. With continued detector development, it is possible to further extend the range of FIR SINS to ultimately bridge the energy gap with available THz *s*-SNOM sources, yet in a single nanospectroscopy instrument. This work highlights the continued advantage of synchrotron radiation as an ultrabroadband coherent light source for near-field nanospectroscopy, especially in the long wavelength regime where alternative low-noise, broadband, quasi-cw laser sources are not readily available.

■ ASSOCIATED CONTENT

📄 Supporting Information

The Supporting Information is available free of charge on the ACS Publications website at DOI: 10.1021/acsphotonics.8b00565.

Detailed description of SINS beamlines at ALS, and additional discussion on detector considerations and modifications for FIR *s*-SNOM (PDF).

■ AUTHOR INFORMATION

Corresponding Authors

*E-mail: habechtel@lbl.gov.

*E-mail: markus.raschke@colorado.edu.

*E-mail: carr@bnl.gov.

ORCID

Omar Khatib: 0000-0002-0721-9684

Markus B. Raschke: 0000-0003-2822-851X

Author Contributions

G.L.C. devised the concept and developed the custom Ge:Cu detector. G.L.C. and H.A.B. performed measurements on SiO₂ test structure and sapphire. O.K. performed measurements on MoS₂, PTCDA, and gate-tuned graphene device, and

subsequent data processing. All coauthors discussed the manuscript, prepared by M.B.R. and O.K. G.L.C., M.B.R., and M.C.M. supervised the project.

Notes

The authors declare no competing financial interest.

ACKNOWLEDGMENTS

M.B.R. acknowledges support from the NSF Science and Technology Center on Real-Time Functional Imaging under DMR-1548924 for development of FIR s-SNOM, and the U.S. Department of Energy, Office of Basic Sciences, Division of Material Sciences and Engineering, under Award No. DE-SC0008807 for the graphene device application. NSLS-II is supported by the U.S. Department of Energy under contract No. DE-SC0012704. The Advanced Light Source is supported by the Director, Office of Science, Office of Basic Energy Sciences, of the U.S. Department of Energy under contract No. DE-AC02-05CH11231. O.K. acknowledges support from the ALS Postdoctoral Fellowship program. The authors thank Sheng Wang and Feng Wang for providing a functional graphene device, and Sam Berweger for preparing exfoliated flakes of MoS₂.

REFERENCES

- (1) Zenhausern, F.; Martin, Y.; Wickramasinghe, H. K. Scanning interferometric apertureless microscopy: Optical imaging at 10 angstrom resolution. *Science* **1995**, *269*, 1083.
- (2) Knoll, B.; Keilmann, F. Near-field probing of vibrational absorption for chemical microscopy. *Nature* **1999**, *399*, 134.
- (3) Taubner, T.; Hillenbrand, R.; Keilmann, F. Performance of visible and mid-infrared scattering-type near-field optical microscopes. *J. Microsc.* **2003**, *210*, 311–314.
- (4) Atkin, J. M.; Berweger, S.; Jones, A. C.; Raschke, M. B. Nano-optical imaging and spectroscopy of order, phases, and domains in complex solids. *Adv. Phys.* **2012**, *61*, 745–842.
- (5) Muller, E. A.; Pollard, B.; Bechtel, H. A.; van Blerkom, P.; Raschke, M. B. Infrared vibrational nanocrystallography and nano-imaging. *Sci. Adv.* **2016**, *2*, e1601006.
- (6) Pollard, B.; Muller, E. A.; Hinrichs, K.; Raschke, M. B. Vibrational nano-spectroscopic imaging correlating structure with intermolecular coupling and dynamics. *Nat. Commun.* **2014**, *5*, 3587.
- (7) Wu, C.-Y.; Wolf, W. J.; Levartovsky, Y.; Bechtel, H. A.; Martin, M. C.; Toste, F. D.; Gross, E. High-spatial-resolution mapping of catalytic reactions on single particles. *Nature* **2017**, *541*, 511–515.
- (8) Qazilbash, M. M.; Brehm, M.; Chae, B.-G.; Ho, P.-C.; Andreev, G. O.; Kim, B.-J.; Yun, S. J.; Balatsky, A. V.; Maple, M. B.; Keilmann, F.; Kim, H.-T.; Basov, D. N. Mott transition in VO₂ revealed by infrared spectroscopy and nano-imaging. *Science* **2007**, *318*, 1750.
- (9) McLeod, A. S.; van Heumen, E.; Ramirez, J. G.; Wang, S.; Saerbeck, T.; Guenon, S.; Goldflam, M.; Anderegg, L.; Kelly, P.; Mueller, A.; Liu, M. K.; Schuller, Ivan K.; Basov, D. N. Nanotextured phase coexistence in the correlated insulator V₂O₃. *Nat. Phys.* **2016**, *13*, 80–86.
- (10) Fei, Z.; Rodin, A. S.; Andreev, G. O.; Bao, W.; McLeod, A. S.; Wagner, M.; Zhang, L. M.; Zhao, Z.; Thiemens, M.; Dominguez, G.; Fogler, M. M.; Neto, A. H. C.; Lau, C. N.; Keilmann, F.; Basov, D. N. Gate-tuning of graphene plasmons revealed by infrared nano-imaging. *Nature* **2012**, *487*, 82–85.
- (11) Chen, J.; Badioli, M.; Alonso-Gonzalez, P.; Thongrattanasiri, S.; Huth, F.; Osmond, J.; Spasenovic, M.; Centeno, A.; Pesquera, A.; Godignon, P.; Elorza, A. Z.; Camara, N.; Garcia de Abajo, F. J.; Hillenbrand, R.; Koppens, F. H. L. Optical nano-imaging of gate-tunable graphene plasmons. *Nature* **2012**, *487*, 77–81.
- (12) Dai, S.; Fei, Z.; Ma, Q.; Rodin, A. S.; Wagner, M.; McLeod, A. S.; Liu, M. K.; Gannett, W.; Regan, W.; Watanabe, K.; Taniguchi, T.; Thiemens, M.; Dominguez, G.; Castro Neto, A. H.; Zettl, A.

Keilmann, F.; Jarillo-Herrero, P.; Fogler, M. M.; Basov, D. N. Tunable phonon polaritons in atomically thin van der Waals crystals of boron nitride. *Science* **2014**, *343*, 1125.

- (13) Basov, D. N.; Fogler, M. M.; Garcia de Abajo, F. J. Polaritons in van der Waals materials. *Science* **2016**, *354*, aag1992.

- (14) Yang, H. U.; Hebestreit, E.; Josberger, E. E.; Raschke, M. B. A cryogenic scattering-type scanning near-field optical microscope. *Rev. Sci. Instrum.* **2013**, *84*, 023701.

- (15) Wagner, M.; McLeod, A. S.; Maddox, S. J.; Fei, Z.; Liu, M.; Averitt, R. D.; Fogler, M. M.; Bank, S. R.; Keilmann, F.; Basov, D. N. Ultrafast dynamics of surface plasmons in InAs by time-resolved infrared nanospectroscopy. *Nano Lett.* **2014**, *14*, 4529–4534.

- (16) Eisele, M.; Cocker, T. L.; Huber, M. A.; Plankl, M.; Viti, L.; Ercolani, D.; Sorba, L.; Vitiello, M. S.; Huber, R. Ultrafast multi-terahertz nano-spectroscopy with sub-cycle temporal resolution. *Nat. Photonics* **2014**, *8*, 841–845.

- (17) Atkin, J. M.; Sass, P. M.; Teichen, P. E.; Eaves, J. D.; Raschke, M. B. Nanoscale probing of dynamics in local molecular environments. *J. Phys. Chem. Lett.* **2015**, *6*, 4616–4621.

- (18) Dönges, S. A.; Khatib, O.; O'Callahan, B. T.; Atkin, J. M.; Park, J. H.; Cobden, D.; Raschke, M. B. Ultrafast nanoimaging of the photoinduced phase transition dynamics in VO₂. *Nano Lett.* **2016**, *16*, 3029–3035.

- (19) Lai, K.; Ji, M. B.; Leindecker, N.; Kelly, M. A.; Shen, Z. X. Atomic-force-microscope-compatible near-field scanning microwave microscope with separated excitation and sensing probes. *Rev. Sci. Instrum.* **2007**, *78*, 063702.

- (20) Huber, A. J.; Keilmann, F.; Wittborn, J.; Aizpurua, J.; Hillenbrand, R. Terahertz near-field nanoscopy of mobile carriers in single semiconductor nanodevices. *Nano Lett.* **2008**, *8*, 3766–3770.

- (21) Liu, M.; Sternbach, A. J.; Basov, D. N. Nanoscale electro-dynamics of strongly correlated quantum materials. *Rep. Prog. Phys.* **2017**, *80*, 014501.

- (22) Falconer, R. J.; Zakaria, H. A.; Fan, Y. Y.; Bradley, A. P.; Middelberg, A. P. J. Far-infrared spectroscopy of protein higher-order structures. *Appl. Spectrosc.* **2010**, *64*, 1259–1264.

- (23) Huth, F.; Govyadinov, A.; Amarie, S.; Nuansing, W.; Keilmann, F.; Hillenbrand, R. Nano-FTIR absorption spectroscopy of molecular fingerprints at 20nm spatial resolution. *Nano Lett.* **2012**, *12*, 3973–3978.

- (24) Degl'Innocenti, R.; Wallis, R.; Wei, B.; Xiao, L.; Kindness, S. J.; Mitrofanov, O.; Braeuninger-Weimer, P.; Hofmann, S.; Beere, H. E.; Ritchie, D. A. Terahertz nanoscopy of plasmonic resonances with a quantum cascade laser. *ACS Photonics* **2017**, *4*, 2150.

- (25) von Ribbeck, H.-G.; Brehm, M.; van der Weide, D. W.; Winnerl, S.; Drachenko, O.; Helm, M.; Keilmann, F. Spectroscopic THz near-field microscope. *Opt. Express* **2008**, *16*, 3430–3438.

- (26) Moon, K.; Do, Y.; Lim, M.; Lee, G.; Kang, H.; Park, K.-S.; Han, H. Quantitative coherent scattering spectra in apertureless terahertz pulse near-field microscopes. *Appl. Phys. Lett.* **2012**, *101*, 011109.

- (27) Kurihara, T.; Yamaguchi, K.; Watanabe, H.; Nakajima, M.; Suemoto, T. Dielectric probe for scattering-type terahertz scanning near-field optical microscopy. *Appl. Phys. Lett.* **2013**, *103*, 151105.

- (28) Kuschewski, F.; von Ribbeck, H.-G.; Döring, J.; Winnerl, S.; Eng, L. M.; Kehr, S. C. Narrow-band near-field nanoscopy in the spectral range from 1.3 to 8.5THz. *Appl. Phys. Lett.* **2016**, *108*, 113102.

- (29) Lang, D.; Döring, J.; Nörenberg, T.; Butykai, Á.; Kézsmárki, I.; Schneider, H.; Winnerl, S.; Helm, M.; Kehr, S. C.; Eng, L. M. Infrared nanoscopy down to liquid helium temperatures. *Rev. Sci. Instrum.* **2018**, *89*, 033702.

- (30) Bechtel, H. A.; Muller, E. A.; Olmon, R. L.; Martin, M. C.; Raschke, M. B. Ultrabroadband infrared nanospectroscopic imaging. *Proc. Natl. Acad. Sci. U. S. A.* **2014**, *111*, 7191–7196.

- (31) Amarie, S.; Keilmann, F. Broadband-infrared assessment of phonon resonance in scattering-type near-field microscopy. *Phys. Rev. B: Condens. Matter Mater. Phys.* **2011**, *83*, 045404.

- (32) Kitamura, R.; Pilon, L.; Jonasz, M. Optical constants of silica glass from extreme ultraviolet to far infrared at near room temperature. *Appl. Opt.* **2007**, *46*, 8118–8133.

- (33) Schubert, M.; Tiwald, T. E.; Herzinger, C. M. Infrared dielectric anisotropy and phonon modes of sapphire. *Phys. Rev. B: Condens. Matter Mater. Phys.* **2000**, *61*, 8187–8201.
- (34) Zhang, X.; Qiao, X.-F.; Shi, W.; Wu, J.-B.; Jiang, D.-S.; Tan, P.-H. Phonon and raman scattering of two-dimensional transition metal dichalcogenides from monolayer, multilayer to bulk material. *Chem. Soc. Rev.* **2015**, *44*, 2757–2785.
- (35) Yu Kobitski, A.; Scholz, R.; Zahn, D. R. T. Theoretical studies of the vibrational properties of the 3,4,9,10-perylene tetracarboxylic dianhydride (PTCDA) molecule. *J. Mol. Struct.: THEOCHEM* **2003**, *625*, 39–46.
- (36) Gerber, J. A.; Berweiger, S.; O'Callahan, B. T.; Raschke, M. B. Phase-resolved surface plasmon interferometry of graphene. *Phys. Rev. Lett.* **2014**, *113*, 055502.
- (37) Woessner, A.; Lundeberg, M. B.; Gao, Y.; Principi, A.; Alonso-González, P.; Carrega, M.; Watanabe, K.; Taniguchi, T.; Vignale, G.; Polini, M.; Hone, J.; Hillenbrand, R.; Koppens, F. H. L. Highly confined low-loss plasmons in graphene-boron nitride heterostructures. *Nat. Mater.* **2015**, *14*, 421.
- (38) Ni, G. X.; Wang, L.; Goldflam, M. D.; Wagner, M.; Fei, Z.; McLeod, A. S.; Liu, M. K.; Keilmann, F.; özyilmaz, B.; Castro Neto, A. H.; Hone, J.; Fogler, M. M.; Basov, D. N. Ultrafast optical switching of infrared plasmon polaritons in high-mobility graphene. *Nat. Photonics* **2016**, *10*, 244.
- (39) Srivastava, G. P., Shind, S. L., Eds. *Length-Scale Dependent Phonon Interactions*; Springer: New York, NY, 2014.
- (40) Basov, D. N.; Averitt, R. D.; van der Marel, D.; Dressel, M.; Haule, K. Electrodynamics of correlated electron materials. *Rev. Mod. Phys.* **2011**, *83*, 471–541.
- (41) Sakanoue, T.; Siringhaus, H. Band-like temperature dependence of mobility in a solution-processed organic semiconductor. *Nat. Mater.* **2010**, *9*, 736.
- (42) García de Abajo, F. J. Graphene plasmonics: Challenges and opportunities. *ACS Photonics* **2014**, *1*, 135–152.
- (43) Low, T.; Avouris, P. Graphene plasmonics for terahertz to mid-infrared applications. *ACS Nano* **2014**, *8*, 1086–1101.
- (44) Narimanov, E. E.; Kildishev, A. V. Metamaterials: Naturally hyperbolic. *Nat. Photonics* **2015**, *9*, 214.
- (45) Santavica, D. F.; Annunziata, A. J.; Reese, M. O.; Frunzio, L.; Prober, D. E. A far-infrared Fourier transform spectrometer with an antenna-coupled niobium bolometer. *Supercond. Sci. Technol.* **2007**, *20*, S398.
- (46) Gaal, P.; Raschke, M. B.; Reimann, K.; Woerner, M. Measuring optical frequencies in the 0–40 THz range with non-synchronized electro-optic sampling. *Nat. Photonics* **2007**, *1*, 577.